# INTERNATIONAL JOURNAL OF ENERGY STUDIES

e-ISSN: 2717-7513 (ONLINE); homepage: https://dergipark.org.tr/en/pub/ijes


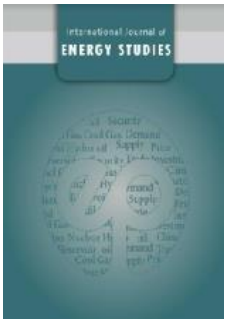



Research Article

Int J Energy Studies, 2020;5(1):13-41

**Received:** 05 June 2020
**Revised:** 15 June 2020
**Accepted:** 16 June 2020


# Assessment of Combustion and Emission Characteristics of Various Gas Mixtures under Different Combustion Techniques


Harun Yılmaz[a,*]

[a]*Department of Airframes and Powerplants, Ali Cavit Çelebioğlu Civil Aviation College, Erzincan Binali Yıldırım University, ORCID:0000-0003-1657-4079*

*(*Corresponding Author:hyilmaz@erzincan.edu.tr)*


**Highlights**

- 2D axisymmetric models of a laboratory scale combustor were constructed
- Flames of $CH_4/CO/H_2/C_2H_6/CO_2/N_2$ blends were simulated
- Oxy-fuel, flameless, and oxy-flameless combustion techniques were investigated
- Tested gas compositions didn't show any gas composition dependence


**You can cite this article as:** Yılmaz, H. "Assessment of Combustion and Emission Characteristics of Various Gas Mixtures under Different Combustion Techniques", *International Journal of Energy Studies* 2020:5(1);13-41


## ABSTRACT


In this study, flame characteristics of 50%CO-50%$H_2$, 80%$CH_4$-10%$C_2H_6$-10%$N_2$ and 40%CO-40%$H_2$-20%$CO_2$ blends under different combustion techniques, namely; oxy-fuel combustion, flameless distributed combustion and oxy-flameless distributed combustion, were investigated using ANSYS Fluent CFD code. Such combustion techniques were employed through replacing combustion air with high $O_2$ content (above 21%) $O_2/CO_2$ mixture, low $O_2$ content (below 21%) $O_2/CO_2$ mixture, and diluting combustion air with 90% $N_2$/10% $CO_2$ mixture to simulate controlled involvement of post combustion gases, respectively. Initially, 2D axisymmetric model of an experimentally tested combustor was utilized to model $CH_4$/air combustion so as to validate applicability of the numerical tool. Later on, premixed combustion of 50%CO-50%$H_2$, 80%$CH_4$-10%$C_2H_6$-10%$N_2$ and 40%CO-40%$H_2$-20%$CO_2$ mixtures was simulated at 2 kW thermal load, 0.8 equivalence ratio and 1.0 swirl number to evaluate effects of oxidizing atmosphere on combustion and emission characteristics, and to determine gas composition dependence of studied combustion techniques. Results showed that temperature, reaction rate and species profiles are similar in trend regardless of the gas composition and oxidizing atmosphere. This indicates gas composition versatility of studied combustion regimes. Additionally, positive impacts of increased turbulent mixing with $O_2$ dilution (increased Re) dominate reaction rates at and near burner outlet, however $O_2$ enrichment effects prevail further downstream.



***Keywords:*** *Oxy-fuel combustion, flameless distributed combustion, oxy-flameless distributed combustion*

## 1. INTRODUCTION

Stringent emission regulations led researchers to seek combustion techniques that can reduce or eliminate pollutants and require minimal retrofit on existing combustion systems, while maintaining desired thermal field. Oxy-fuel combustion is one of these techniques in which fuel molecules are oxidized by pure $O_2$ or a mixture of $O_2$ and $CO_2$ (or a mixture of $O_2$ and $H_2O$) [1]. Consequently, $CO_2$ and water vapor constitute majority of combustion products [2] and this situation, thereafter, enables cost efficient carbon capture and sequestration with reduced or no $NO_x$ [1]. Oxy-fuel applications produce very high flame temperatures and have the advantages of improved thermal efficiency, decreased volume of combustion products, and increased potentiality for reducing pollutants at higher $O_2$ concentrations [3]. High flame temperature is needed for chain reactions to progress. However, material properties of both upstream and downstream components limit temperature increment (dissociation may also occur at elevated temperatures). So, minimum amount of $O_2$ in oxidizer mixture must be ensured to achieve a stable flame under oxy-fuel combustion conditions [4]. Additionally, Abubakar et al. reported that oxygen amount in post combustion gases must be lower than 50 ppm not to cause corrosion in ducts and reactions with $CO_2$ in reservoirs [5]. The contaminants in flue gas stream that mainly result from excess oxygen, incomplete combustion products and residual $N_2$ and Ar give rise to energy consumption of $CO_2$ capture process, and so efficiency of the overall system reduces [6]. Because, air separation, $O_2$ production, exhaust gas recirculation, $CO_2$ capture and condensation require energy [7]. Another disadvantage of high level of $O_2$ is that flame may manifest upstream and cause flashback due to high flame speed (in premixed systems) [1]. Regarding these issues and the facts that lean-premixed combustion systems are associated with reduced temperatures (and $NO_x$ levels), oxidizer is a mixture of $CO_2$ and $O_2$ in oxy-fuel combustion (almost no $N_2$), and air separation consumes energy; stoichiometric or near stoichiometric conditions are desirable for oxy-flame stability and lower operational costs [2, 5-6].

Replacing $N_2$ in oxidizer mixture with $CO_2$ has significant impacts on flame characteristics. Because, $CO_2$ has typical properties such as weaker thermal diffusion ability and higher thermal capacity compared to $N_2$ [4]. $CO_2$ also affects chemical kinetics [8, 9] and the amount of heat transferred through radiation [10]. As above mentioned properties of $CO_2$ vary flame temperature, $CO_2$ predominates flame characteristics. At sufficiently high $CO_2$ fractions, burning velocity (hence effectiveness of combustion process) decreases, and this modifies species and temperature distributions within the combustion chamber [4]. Furthermore, flame stability improves with $CO_2$

addition because of the turbulent mixing rate improvement [10]. Therefore, optimum $CO_2$ amount in oxidizer must be determined depending on the operating conditions and gas composition.

In literature, there are many studies addressing oxy-combustion characteristics of gaseous and solid fuels. Shakeel et al. simulated oxy-$CH_4$ combustion in a model GT (gas turbine) combustor to find optimum radiation model and reaction mechanism that can successfully reproduce characteristics of such flames. To that end, they compared 3 different $CH_4$/air reaction mechanisms and radiation models. They also examined effects of $CO_2$ content of oxidizer, equivalence ratio and thermal input. They concluded a set of most appropriate combustion mechanism and radiation model that can capture flame anchoring position, and showed that $CO_2$ addition and thermal input increments increase emissions of CO [11]. Imteyaz et al. experimentally investigated stable operating range, and flashback and blowout equivalence ratios of hydrogen enriched oxy-$CH_4$ flames in a model GT combustor by varying hydrogen amount, and total mass flow rate of both reactants and oxidants (to understand flow field effects). They demonstrated that stability limits shift to fuel lean conditions with increasing hydrogen amount. Although decreased Re indicates less turbulence and flame velocity, this movement was attributed to improved reaction-kinetics [12]. As mentioned, oxy-fuel combustion has unconventional heat transfer (through radiation) properties. Ditaranto and Oppelt conducted an experimental study on oxy-$CH_4$ flames to measure the amount of heat transferred through radiation from the axis of the flame at different $O_2$ fractions. They reported that maximum value of heat flux increases and the area of maximum heat flux occurrence moves upstream with $O_2$ increments, and radiative behaviors of conventional air and 35% $O_2$/$CO_2$ mixture are similar in distribution [13]. Li et al. experimentally studied effects of $CO_2$ on oxy-fuel catalytic combustion of hydrogen in a channel of millimeter scale by giving special attention to the amount of heat transfer, reactivity and the interaction between homogenous and heterogenous reactions. In their study, they tested two kinds of reactors (tubular and channel types). They indicated that oxy-fuel reactions can still be maintained at a minimum $O_2$ concentration of 21% in the tubular reactor, when Pt is used as a catalyst. They also showed that $CO_2$ affects ignition characteristics of both homogenous and heterogenous reactions [14].

An alternative combustion technique used to reduce pollutant emissions is flameless combustion, which is also denoted as colorless or flameless distributed combustion [15]. The reason for entitling this technique as “flameless or colorless” is that the area where fuel molecules are oxidized does not exhibit any visual signature and flame front is not apparent when distributed

regime is obtained at an $O_2$ concentration specified by flow field, fuel type, operating conditions etc. [16]. The principle necessities for obtaining this regime include sufficient and prompt mixing between combustion air, fuel species and recycled post combustion products to constitute a reactive mixture with high temperature. This hot (ideally, higher than self-ignition temperature of the mixture [15]) and low oxygen content mixture, later on, simultaneously ignites and promotes to distributed combustion conditions in which reaction zone expands (with reduced reaction rate) within the entire combustion chamber rather than concentrating in a tiny zone near burner outlet [17]. The absence of flame front, which is qualified by high reactivity and sudden temperature increment, causes emissions of $NO_x$ to reduce, eliminates combustion instabilities, and a lean flame with low noise arises [15, 16]. Other benefits of flameless combustion are uniform temperature distribution (since heat is released from the entire volume of the combustor [18]) and reduced pollutant emissions-almost non (uniformity eliminates local hot temperature zones and reduces thermal $NO_x$ [18]). Compared to conventional combustion, temperature increment is at a lesser degree at flameless regime although thermal input is the same. This is because of low oxygen (high dilution) content and elevated temperature of combustible mixture, which reduces reaction rate and leads to a limited temperature rise [17, 19].

Flameless distributed combustion technique has been thoroughly investigated by many researchers. Karyeyen et al. performed experimental studies on $H_2$ enriched $CH_4$ flames. They used a mixture of $N_2$ and $CO_2$ as oxidizer to achieve flameless combustion conditions. Results of respective study showed that minimum $O_2$ requirement of such combustion condition depends on diluent type, and $H_2$ addition reduces this minimum value. Additionally, $NO_x$ emissions were found to significantly reduce at distributed regime, while the trend of emissions of CO depended on diluent type [20]. In another study, Karyeyen and Ilbas numerically examined distributed regime of coal derived syngas flames to investigate $H_2$ enrichment effects on flammability limits and emissions. They stated that temperature uniformity increases and emissions of $NO_x$ decrease, when chemical reactions spread out within the whole combustor volume [21]. In the course of findings mentioned above, it can be said that main impacts of flameless combustion technique are increased uniformity and decreased emissions [22-25].

As noted before, high flame temperatures and high velocity associated with oxy-fuel combustion technique pose challenges for upstream components and flame stability issues by demonstrating that oxidizer mixture needs to be diluted. In oxy-flameless distributed combustion technique, the

oxidizer mixture is composed of $O_2$ and $CO_2$, and distributed combustion can be obtained below a certain $O_2$ level depending on the inlet parameters [26]. This combustion technique is reported to have benefits such as increased static flame stability, reduced CO emissions, and uniform temperature field [27].

In this study, flames of $CH_4/CO/H_2/C_2H_6/CO_2/N_2$ blends were simulated in 2D axisymmetric models of a laboratory scale-premixed-swirl stabilized combustor under different combustion techniques, which are oxy-fuel combustion, flameless distributed combustion and oxy-flameless distributed combustion, to evaluate impacts of oxidizer mixture on combustion and emission properties of such flames, and to determine gas composition dependence of such combustion techniques. First, $CH_4$/air combustion was simulated at a constant thermal power and swirl number (2 kW and 1.0, respectively), and at different equivalence ratios ($\Phi$=0.6, 0.7 and 0.8) to validate applicability of the numerical model. Later on, mixtures of 50% CO – 50% $H_2$, 80% $CH_4$ – 10% $C_2H_6$ – 10% $N_2$ and 40% CO – 40% $H_2$ – 20% $CO_2$ were analyzed in these models under different combustion atmospheres. To obtain flameless distributed combustion conditions, a mixture of $N_2$ and $CO_2$ (90% $N_2$- 10% $CO_2$ – by volume, as they compose bulk of exhaust gases at stoichiometry) was introduced to combustion air (by keeping $O_2$ amount constant) at different quantities to reduce $O_2$ fraction in oxidizer, hence to designate a minimum $O_2$ amount at which distributed combustion is accomplished. Moreover, $CO_2$ and $O_2$ constituted oxidizer mixture for oxy-fuel and oxy-flameless distributed ($O_2$ < 21%) combustion techniques.

## 2. PHYSICAL AND MATHEMATICAL MODELS

### 2.1. Physical Model

In this study, 2D models of an experimentally tested combustor were utilized. Only one-half of the combustor was considered to reduce computational time. The respective, steel made, combustor is 1655 mm in length, and has 320 mm inner and 330 mm outer diameter. Schematic view of the combustor is given in Figure 1. Details of the combustor and combustion system can be found in study of Yilmaz and Yilmaz [28].

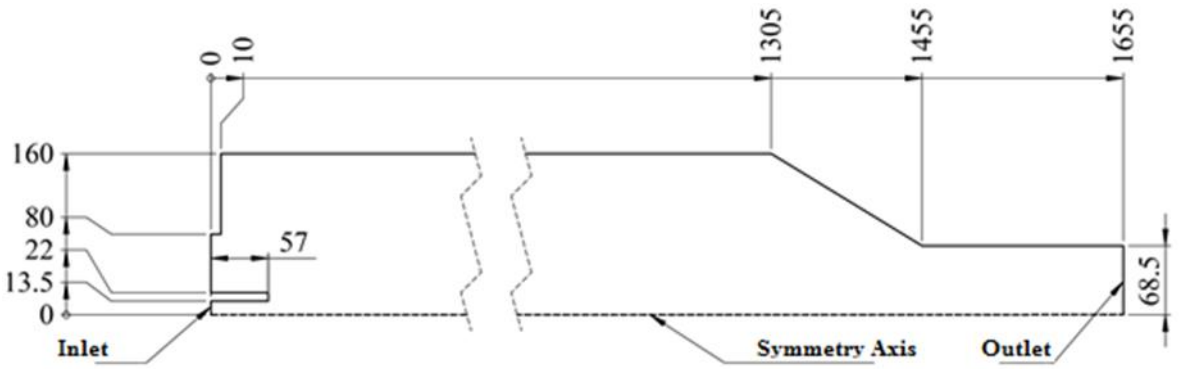


**Figure 1.** Schematic of the combustor (all dimensions are in millimeters)

### 2.2. Mathematical Model

The mathematical model is based on the 2D - steady - axisymmetric forms of continuity, species, conservation of energy and momentum equations which control the flow, chemistry, heat transfer and their interactive relations. These equations are as follows:

*Continuity equation;*

$$\frac{\partial(\rho u)}{\partial x}+\frac{\partial(\rho v r)}{\partial r}=0 \quad (1)$$

*Conservation of momentum;*

$$\frac{\partial(\rho u v)}{\partial x}+\frac{1}{r}\left(\frac{\partial(\rho u v r)}{\partial r}\right)=-\frac{\partial p}{\partial x}+\frac{\partial}{\partial x}\left(\frac{\frac{4}{3}\mu\partial u}{\partial x}\right)+\frac{1}{r}\frac{\partial}{\partial r}\left(r\mu\frac{\partial u}{\partial r}\right)-\frac{\partial}{\partial x}\left(\frac{2\mu}{3r}\frac{\partial \vartheta r}{\partial r}\right)+\frac{1}{r}\frac{\partial}{\partial r}\left(r\mu\frac{\partial \vartheta}{\partial x}\right) \quad (2)$$

*Radial momentum;*

$$\frac{\partial(\rho u v)}{\partial x}+\frac{1}{r}\left(\frac{\partial(\rho v \vartheta r)}{\partial r}\right)=-\frac{\partial p}{\partial r}+\frac{\partial}{\partial x}\left(\mu\frac{\partial u}{\partial x}\right)-\frac{1}{r}\frac{\partial}{\partial r}\left(\frac{2r\mu}{3}\frac{\partial u}{\partial x}\right)+\frac{\partial}{\partial x}\left(\mu\frac{\partial v}{\partial x}\right)+\frac{1}{r}\frac{\partial}{\partial r}\left(\frac{4r\mu}{3}\frac{\partial v}{\partial r}\right)-$$

$$\frac{1}{r}\frac{\partial}{\partial r}\left(\frac{2\mu v}{3}\right) \quad (3)$$

*Energy equation;*

$$\frac{\partial(\rho u h)}{\partial x}+\frac{1}{r}\frac{\partial(\rho v h r)}{\partial r}=\frac{\partial}{\partial x}\left(k\frac{\partial T}{\partial x}\right)+\frac{1}{r}\frac{\partial}{\partial r}\left(k\frac{\partial T}{\partial r}r\right)-\frac{1}{r}\frac{\partial}{\partial r}\left(r\rho\sum_{i=1}^{N}Y_i h_i V_i\right)-\frac{\partial}{\partial x}\left(\rho\sum_{i=1}^{N}Y_i h_i U_i\right)+$$

$$q \quad (4)$$

*Species conservation;*

$$\frac{\partial(\rho u Y_i)}{\partial x}+\frac{1}{r}\frac{\partial(\rho u r Y_i)}{\partial r}=\frac{\partial}{\partial x}\left[D_i\frac{\partial(\rho Y_i)}{\partial x}\right]+\frac{1}{r}\frac{\partial}{\partial r}\left[D_i r\frac{\partial(\rho Y_i)}{\partial r}\right]+wi \quad (5)$$

In these equations: $\rho$, density; $u$ and $v$, velocity; $p$, pressure; $\mu$, dynamic viscosity; $h$, enthalpy; $k$, thermal conductivity; $T$, temperature; $U_i$and $Y_i$, velocity of *i*th specie; $Y_i$, mass fraction of *i*th species; $q$, volumetric heat generation rate; $D_i$, diffusion coefficient of the *i*th species, and $wi$, production rate of the *i*th species [29]. All equations were discretized and solved using second order upwind scheme and finite volume method, respectively. As pressure-based solver is used,

pressure and velocity must be linked for closure of transport equations [2]. So, Coupled algorithm was employed to link velocity and pressure.

For all gas mixtures, one step global reaction mechanisms were used. The interaction between turbulence and chemistry was handled using Eddy Dissipation model (assuming that turbulent mixing limits reaction rate) in which net formation rate of species *i* through chemical reaction $R_i$ ($R_{i,r}$) is calculated by two equations below [30].

$$R_{i,r} = v'_{i,r} M_{w,i} A \rho \frac{\varepsilon}{k} min_{\mathcal{R}} \left( \frac{Y_{\mathcal{R}}}{v'_{\mathcal{R},i} M_{w,\mathcal{R}}} \right) \quad (6)$$

$$R_{i,r} = v'_{i,r} M_{w,i} A B \rho \frac{\varepsilon}{k} \frac{\sum_P Y_P}{\sum_j^N v''_{j,r} M_{w,j}} \quad (7)$$

Where: $v'_{i,r}$, stoichiometric coefficient of species *i* in reaction *r*; N, total number of species; $Y_P$, mass fraction of any product, P; $Y_{\mathcal{R}}$, mass fraction of a specific reactant, R; $M_{w,i}$, molecular weight of species *i*; A (0.4) and B (0.5) are constants [30].

RNG k-ε turbulence model [30] along with swirl dominated flow option was adopted to take turbulence effects on flow into account, as this model was reported by many researchers to be capable of reproducing characteristics of the swirling flows [31-32]. Additionally, P-1 radiation model [30] was used to consider effects of radiation on temperature distribution. Calculation methods of mixture density, specific heat, thermal conductivity and viscosity, and mass diffusivity are as follows; incompressible-ideal-gas, mixing law, ideal-gas-mixing-law, and kinetic theory.

## 3. BOUNDARY AND OPERATING CONDITIONS

An applicable set of boundary conditions were used for numerical model. Velocity inlet and pressure outlet conditions were implemented at inlet and outlet, respectively. Standard conditions (e.g., gauge pressure, 0) were set at the exit of the combustor, and hydraulic diameter and turbulence intensity were specified for both inlet and outlet. Besides, no slip condition was deployed at the interface between solid and gas phases.

Gas mixtures considered in this study are 50% CO – 50% $H_2$, 80% $CH_4$ – 10% $C_2H_6$ – 10% $N_2$ and 40% CO – 40% $H_2$ – 20% $CO_2$. Equivalence ratio (Φ=0.8), swirl number (SN=1.0) and thermal power (2 kW) were kept constant for all gas mixtures. To achieve oxy-fuel and oxy-flameless distributed combustion conditions, combustion air was replaced with a mixture of $O_2$ and $CO_2$, in which $O_2$ concentration was increased from 25% to 50% by a step of 5%, and was

reduced from 19% to 11% by a step of 2%, respectively. Furthermore, nitrogen and $CO_2$ mixture (exhaust gas entrainment) was added to fresh air at different quantities to reduce $O_2$ concentration (from 20 % to 10 by a step of 2%), hence to designate an oxygen concentration at which chemical reactions are distributed to whole combustor volume. Fuel and oxidizer mixtures, of which flow rates of components were calculated depending on the equivalence ratio and thermal load, were assumed to be completely premixed at 300 K, and then combusted. The oxidizer mixtures tested in this study are given in Table 1.

## 4. MESH INDEPENDENCE AND VERIFICATION OF NUMERICAL MODEL

In order to assign a computational domain that comprises of the lowest number of elements for an accurate and least time consuming simulation, numerous mesh structures that have 16584, 20904, 29158, 41310, 62497 or 116820 elements were constructed. By using these grids, $CH_4$/air combustion was modelled at $\Phi$=0.6 and SN=1.0, and predicted temperature values at combustor centerline are presented in Figure 2. Since temperature values do not differ at combustor outlet, outlet section of the combustor (1000-1650 mm) was excluded to better interpret the results. As seen, temperature curves accord in trend for all mesh structures, whereas value differences exist. However, increasing number of elements from 62497 to 116820 doesn't considerably alter temperature distribution. So, mesh structure with 62497 elements was further utilized in this study.

**Table 1.** Oxidizer mixtures.

| Combustion Technique | Oxidizer Mixture (OM) | $O_2$ (%) | $N_2$ (%) | $CO_2$ (%) |
|---|---|---|---|---|
| Oxy-fuel combustion | OM1 | 25 | - | 75 |
| | OM2 | 30 | - | 70 |
| | OM3 | 35 | - | 65 |
| | OM4 | 40 | - | 60 |
| | OM5 | 45 | - | 55 |
| | OM6 | 50 | - | 50 |
| Oxy-flameless distributed combustion | OM7 | 19 | - | 81 |
| | OM8 | 17 | - | 83 |
| | OM9 | 15 | - | 85 |
| | OM10 | 13 | - | 87 |
| | OM11 | 11 | - | 89 |
| Flameless distributed combustion | OM12 | 10 | 84.760 | 5.240 |
| | OM13 | 12 | 83.712 | 4.288 |
| | OM14 | 14 | 82.664 | 3.336 |
| | OM15 | 16 | 81.616 | 2.384 |
| | OM16 | 18 | 80.568 | 1.432 |
| | OM17 | 20 | 79.52 | 0.48 |

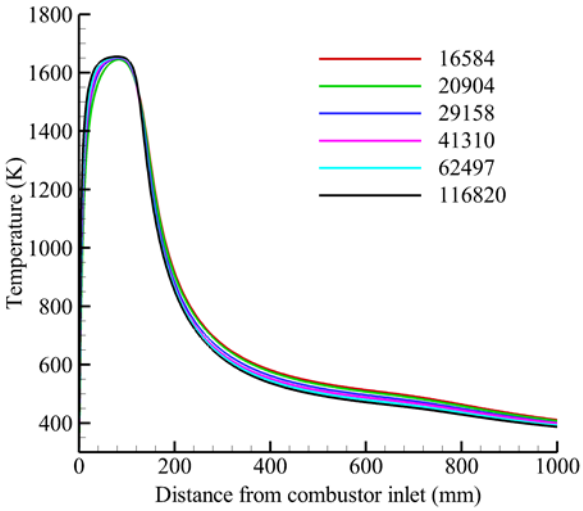


**Figure 2.** Mesh refinement study

The availability of the numerical model was verified using measured temperature values of premixed $CH_4$/air combustion at 2 kW thermal load, 1.0 swirl number and different equivalence ratios (0.6, 0.7 and 0.8) in experimental system described in Ref. [28], and the data was taken from Ref. [33]. These values were compared with predicted temperature values at the same conditions, and a high consistency was obtained by indicating availability of the numerical scheme (Figure 3). As clearly seen, equivalence ratio only alters peak temperature value near burner outlet, and starting from axial distance of about 200 mm from burner outlet, temperature distributions nearly become insensitive to equivalence ratio. However, slight decrements in temperature values appear at combustor outlet because of the modified heat transfer characteristics at different temperatures, and the lowest exit temperature value is at $\Phi$=0.8.

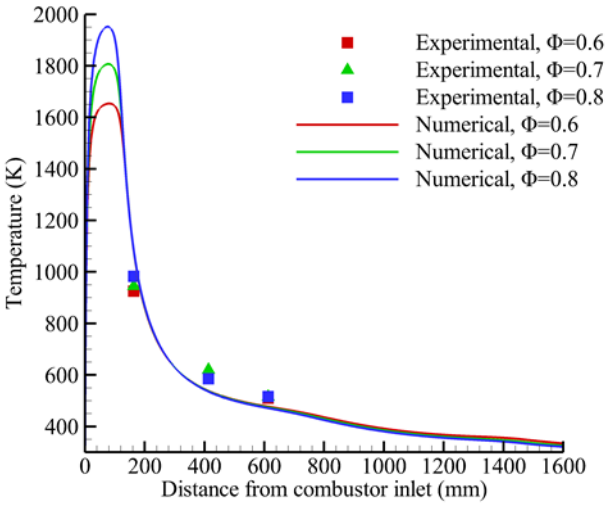


**Figure 3.** Validation of numerical model

## 5. RESULTS AND DISCUSSIONS

Predicted temperature values of 50% CO – 50% $H_2$ mixture at different oxidizer atmospheres ($O_2$ concentration was increased from 25% to 50%, at intervals of 5%, and $CO_2$ amount was varied accordingly) under oxy fuel combustion conditions were plotted against axial distance from burner outlet, and presented in Figure 4. As seen, temperature values sharply increase right after burner outlet irrespective of the $O_2$ amount in oxidizer mixture, and reach their peak at an axial distance of about 170 mm away from burner outlet. Besides, peak temperature values considerably increase with $O_2$ amount in the $O_2$ concentration range of 25%-45%. However, this increment diminishes when $O_2$ concentration is increased from 45% to 50%. The axial range where fuel molecules are oxidized does not significantly vary with $O_2$ concentration. As $O_2$ concentration increases, mass flow rate of reactants reduces. As a result, turbulence intensity and flame speed reduce. But, reaction kinetics improve with $O_2$ enrichment. The competition between these two phenomena is responsible for this slight variation. Starting from of an axial distance of about 200 mm away from burner outlet, lower temperature values form at higher $O_2$ concentrations. This is because of improved heat transfer characteristics (higher radiation intensity) at higher $O_2$ concentrations. At these conditions, flame emissivity increases because of the high levels of $H_2O$ and $CO_2$ in exhaust gas stream, as these gases contribute to radiation [34]. This situation could also be evaluated from another aspect; $CO_2$ modifies chemical kinetics and reduces thermal diffusivity [35]. Consequently, flame length increases at higher $CO_2$ concentrations, as well as downstream temperature values. At the exit sections of the combustor, temperature profiles show a good

agreement both in terms of trend and value. Temperature values nearly become insensitive to axial distance and $O_2$ concentration, and nearly the same exit temperature values occur.

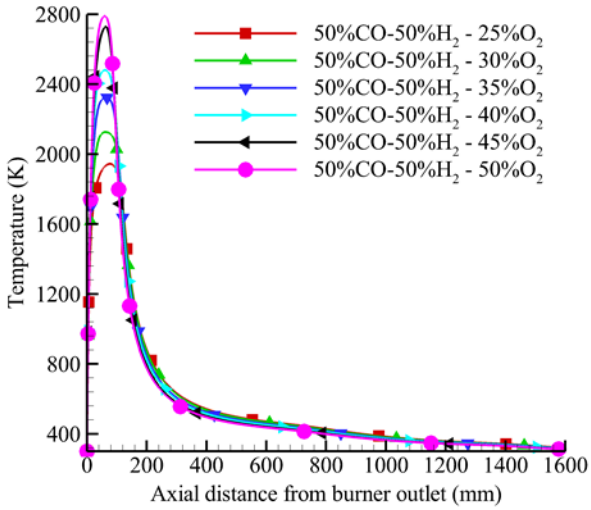


**Figure 4.** Axial temperature profiles of 50% CO – 50% $H_2$ mixture at different $O_2$ concentrations under oxy-fuel combustion conditions

In Figure 5, radial temperature profiles of 50% CO – 50% $H_2$ mixture are illustrated at three different axial locations (50, 150 and 250 mm away from burner outlet). Since radial temperature values do not substantially change with radial distance starting from a certain radial location, these values were plotted in the radial distance range of 0-100 mm. Consistent with axial temperature values, radial temperature values increase with $O_2$ concentration at axial location of 50 mm. Nevertheless, these values steeply decrease as radial distance increases, and starting from a radial location of about 15 mm, temperature values are affected by neither $O_2$ concentration nor radial distance. At axial location of 150 mm, the difference in peak temperature values decreases, and an opposite behaviour is observed. At this axial location, the highest temperature value form at the lowest $O_2$ concentration (mainly because of the increased flame length). Further increment in radial distance doesn't largely alter temperature distribution. At 250 mm axial location, radial temperature profiles exhibit a significant dependence on $O_2$ concentration. Radial temperature values decrease as $O_2$ concentration (this correlates with the study of Ref. [4] in which it was stated that oxy-fuel flames exhibit lower expansion in radial direction) and radial distance increase, and the difference between radial temperature values become more distinct. Furthermore, the radial range in which temperature values reduce widens with axial distance, and temperature decrement

becomes more linear. Effects of flame elongation on radial temperature distribution at elevated $CO_2$ concentrations can clearly be seen in Figure 6.

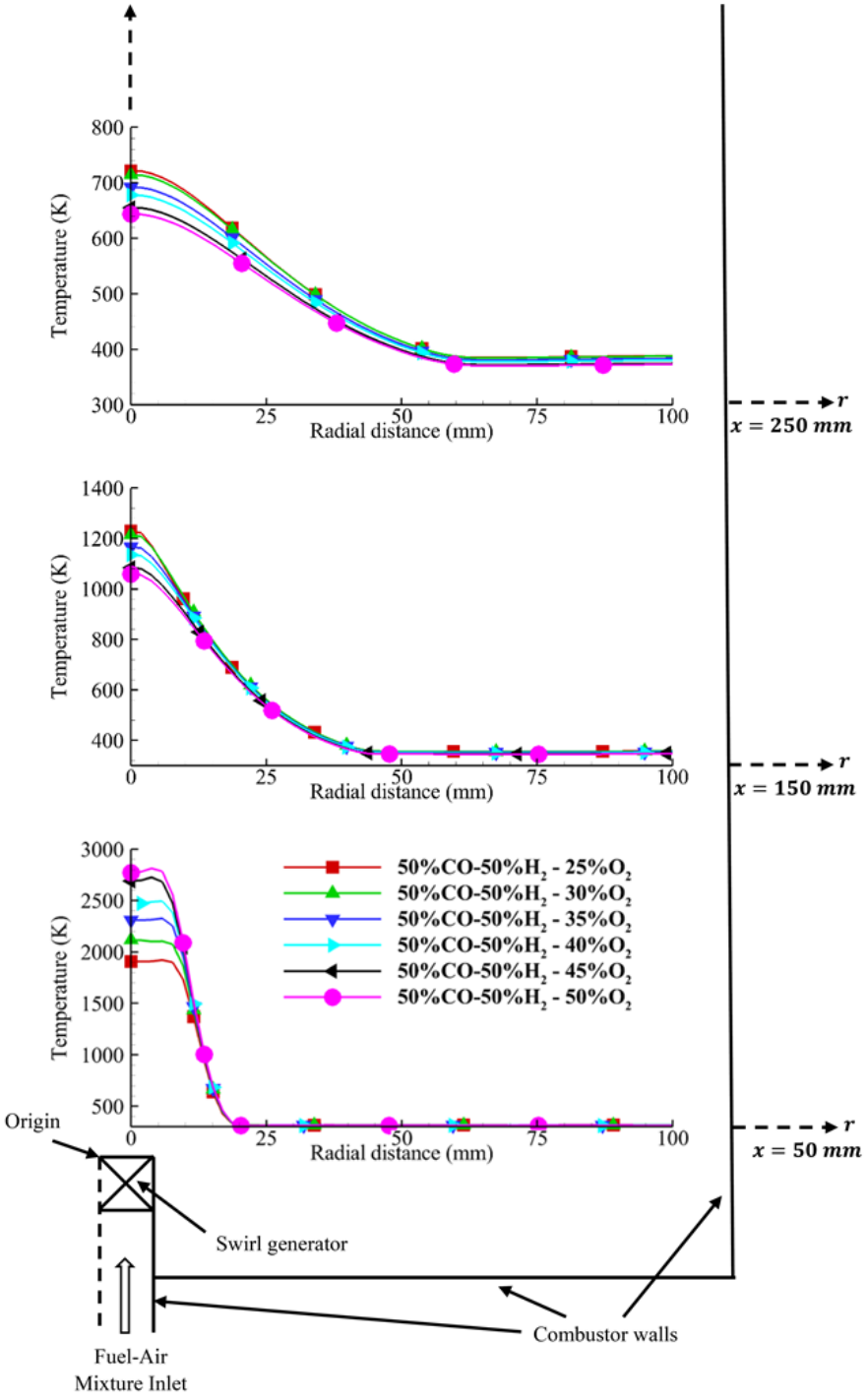


**Figure 5.** Radial temperature profiles of 50% CO – 50% $H_2$ mixture under oxy-fuel combustion conditions

In Figure 7, turbulent rate of reaction profiles of 50% CO – 50% $H_2$ mixture are presented. As stated earlier, reduction in Reynolds number results with lower mixing intensity between fuel and oxidizer molecules, and slower flame speed. Contrarily, reaction kinetics increase at elevated $O_2$ levels. At burner outlet, turbulent rate of reaction is the highest when $O_2$ concentration is the lowest, and it decreases with $O_2$ addition. This situation indicates that adverse impacts of Reynolds number decrement on reaction kinetics are more profound than beneficial impacts of $O_2$ addition at inlet sections of the combustion chamber. On the other hand, starting from an axial distance of about 10 mm, beneficial impacts of $O_2$ addition on turbulent rate of reaction predominate, and slightly higher reaction rates are present at $O_2$ rich conditions.

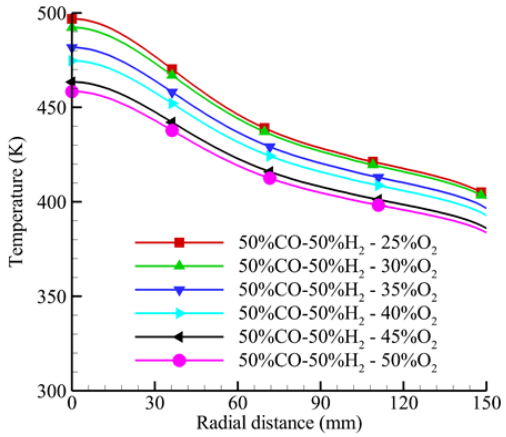


**Figure 6.** Radial temperature profiles of 50% CO – 50% $H_2$ mixture at 500 mm axial location

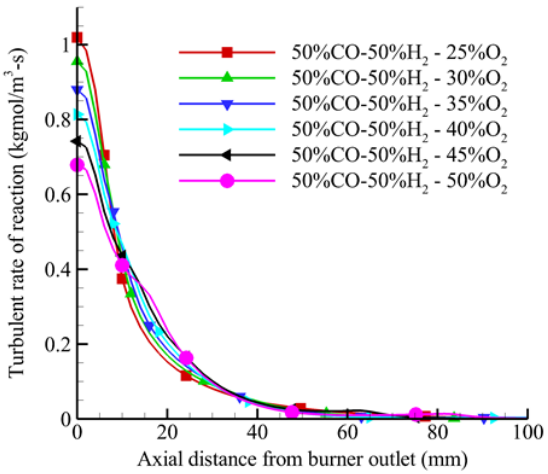


**Figure 7.** Turbulent rate of reaction profiles of of 50% CO – 50% $H_2$ mixture under oxy-fuel combustion conditions

$H_2$ and $H_2O$ mass fraction profiles of 50% CO – 50% $H_2$ mixture show a good compliance with reaction rate profiles. Compared to the case in which $O_2$ concentration is 50%, consumption of $H_2$ molecules is slightly faster near burner inlet at 25% $O_2$ concentration. However, it slows down further downstream, and becomes lower than that of at 50% $O_2$ concentration. When $O_2$ concentration is 50%, $H_2$ is completely consumed at axial distance of about 60 mm. Moreover, formation of $H_2O$ molecules is faster at 50% $O_2$ concentration irrespective of the axial location (Figure 8).

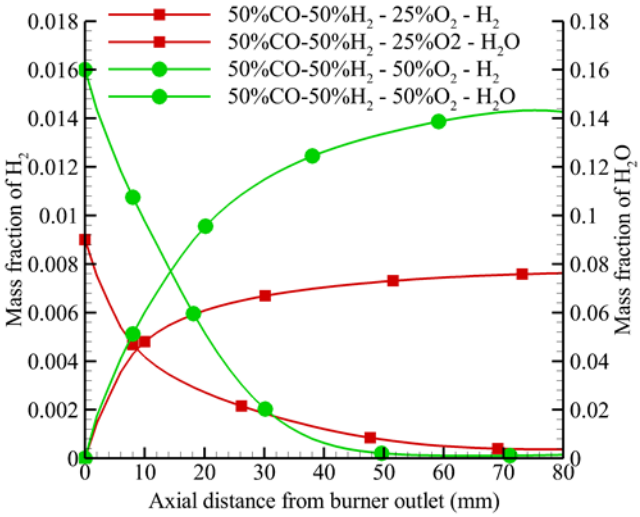


**Figure 8.** $H_2$ and $H_2O$ mass fraction profiles of 50% CO – 50% $H_2$ mixture at 25% and 50% $O_2$ concentrations

When mixtures of 80% $CH_4$ – 10% $C_2H_6$ – 10% $N_2$ and 40% CO – 40% $H_2$ – 20% $CO_2$ were combusted under the same oxy-fuel combustion conditions, the trend of temperature profiles and their dependence on $O_2$ content throughout the combustion chamber don't vary. Temperature profiles show similar behavior to that of 50%CO-50%$H_2$ mixture. 80% $CH_4$ – 10% $C_2H_6$ – 10% $N_2$ and 40% CO – 40% $H_2$ – 20% $CO_2$ mixtures form different peak temperature values depending on heat capacities' (Figure 9). This situation is the evidence of gas composition diversity of oxy-fuel combustion technique. As species profiles (such as; CO, $CO_2$, $H_2$, $H_2O$, $CH_4$, $C_2H_6$) show a good consistency in behavior with temperature and reaction rate profiles based on the $O_2$ amount, species distributions of 80% $CH_4$ – 10% $C_2H_6$ – 10% $N_2$ and 40% CO – 40% $H_2$ – 20% $CO_2$ mixtures will not be plotted against distance from burner outlet, and effects of $O_2$ amount on these parameters will not be addressed in this study.

As mentioned before, key prerequisite to achieve flameless distributed combustion regime is proper mixing of fresh fuel/air mixture with hot combustion products (dilution) so that initiation of chemical reactions are retarded until appropriate mixing is obtained and reaction zone is expanded. This outspread mixture is then heated up above self-ignition temperature for combustion to simultaneously start. In flameless combustion regime, pollutant emissions and adiabatic flame temperature decrease, as formation of an intensified reaction zone is prevented [18]. Yet, Khalil and Gupta concluded that dilution temperature (preheating) has a minimal impact on reaction zone distribution and emissions [16]. So, similar to studies of Ref. [19, 26, 36], it was assumed that there is no preheating and mixture temperature is 300 K in this study.

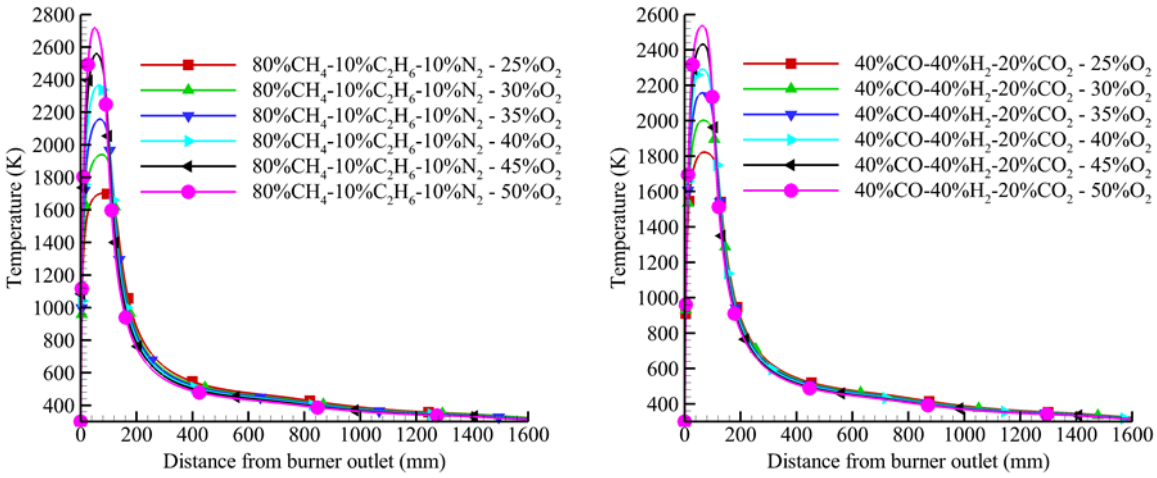


**a)** **b)**

**Figure 9.** Axial temperature profiles of; a) 80% $CH_4$ – 10% $C_2H_6$ – 10% $N_2$, b) 40% CO – 40% $H_2$ – 20% $CO_2$ mixtures under oxy fuel combustion conditions

At this part of the study, $O_2$ concentration was reduced from 20% to 10% (at intervals of 2%) to seek flameless distributed combustion conditions. For this purpose, right amount of conventional air (21%$O_2$-79%$N_2$), which is needed for complete combustion at 0.8 equivalence ratio, was mixed with 10%$CO_2$-90%$N_2$ mixture to reduce $O_2$ concentration (fuel and air flow rates were kept constant, while flow rate of 10%$CO_2$-90%$N_2$ mixture was increased accordingly).

In Figure 10, axial temperature profiles of 80% $CH_4$ – 10% $C_2H_6$ – 10% $N_2$ mixture at different $O_2$ concentrations are demonstrated. In the case of combustion in higher $O_2$ fractions, peak temperature values are very high, and these values are directly proportional to $O_2$ amount. At these

conditions, temperature values sharply increase and then decrease. However, the axial range in which temperature values peak widens as $O_2$ concentration decreases. This range is the highest at 10% $O_2$ concentration, which is the evidence that reaction zone has spread within the combustion chamber. Although the difference in calculated peak temperature values at 10% and 20% $O_2$ concentrations is over 600 K, downstream (200-1600 mm) temperature values are higher and thermal field is more uniform at 10% $O_2$ concentration (temperature profiles are nearly inline at 10% and 12% $O_2$ concentrations). Additionally, calculated uniformity index [30] values at 10%, 12% and 20% $O_2$ concentrations are 0.9665, 0.9645 and 0.9645, respectively. In the view of above mentioned findings, it can be concluded that distributed regime can be obtained at 10% $O_2$ concentration at these conditions.

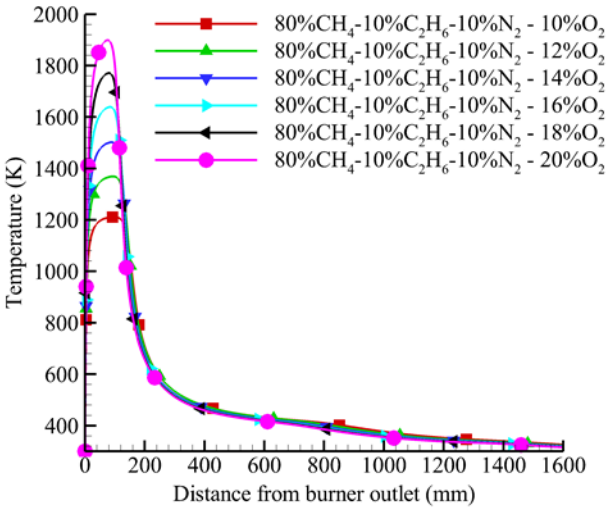


**Figure 10.** Axial temperature profiles of 80% $CH_4$ – 10% $C_2H_6$ – 10% $N_2$ mixture at different $O_2$ concentrations

In the flame region (at axial location of 50 mm), effects of $O_2$ concentration on flame temperature are very significant. Flame temperatures promptly decrease in the radial distance range of 0-20 mm, and then stabilize at nearly the same value in the entire radial range irrespective of the $O_2$ concentration. At 150 mm axial location, radial temperature values at 10% $O_2$ concentration are slightly higher than that of at 20% $O_2$ concentration in the radial distance range of 0-10 mm. But, these values are higher at 20% $O_2$ concentration in the radial distance range of 10-40 mm. Out of this radial range, temperature values are not affected by radial distance. Although flame temperature values are very low at 10% $O_2$ concentration, radial temperature values are very close

in both flame region and outside the flame region at 250 mm axial location. This proximity increases, as axial distance increases (Figure 11).

In a combustion process, nitrogen oxides form via there different mechanisms. Since there is no fuel-bound nitrogen, fuel NO mechanism was excluded in this study, while prompt (also called Fenimore mechanism) and thermal $NO_x$ formation mechanisms were considered. When flame temperature and residence time are low, and fuel rich conditions are present, prompt NO mechanism governs $NO_x$ formation. The latter is highly temperature dependent, as expected [21]. In Figure 12, axial $NO_x$ profiles along the centreline of the combustor are presented. As axial $NO_x$ values excessively increase with $O_2$ amount, i.e., temperature increase, axial $NO_x$ profiles are given in two separate figures to better evaluate the results. As clearly seen, thermal Zeldovich mechanism dominates $NO_x$ formation. Additionally, O and OH concentrations and also residence time increase, as $O_2$ amount increases. Hence, $NO_x$ increases. However, emitted $NO_x$ levels are very low at 10% and 12% $O_2$ concentrations, and nearly zero $NO_x$ is emitted at 10% $O_2$ concentration by pointing out that flameless combustion conditions are achieved.

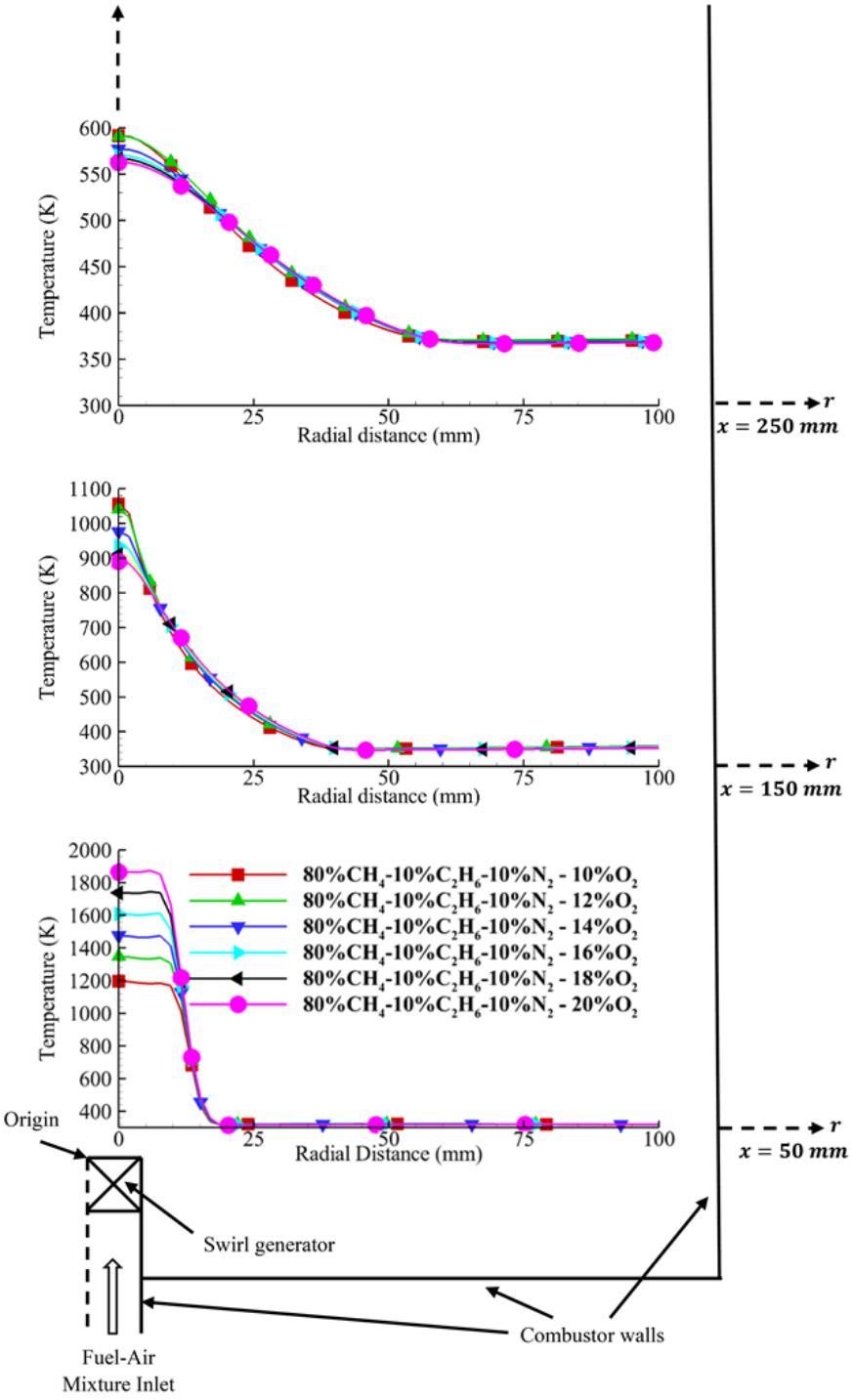


**Figure 11.** Radial temperature profiles of 80% $CH_4$ – 10% $C_2H_6$ – 10% $N_2$ mixture at different $O_2$ concentrations

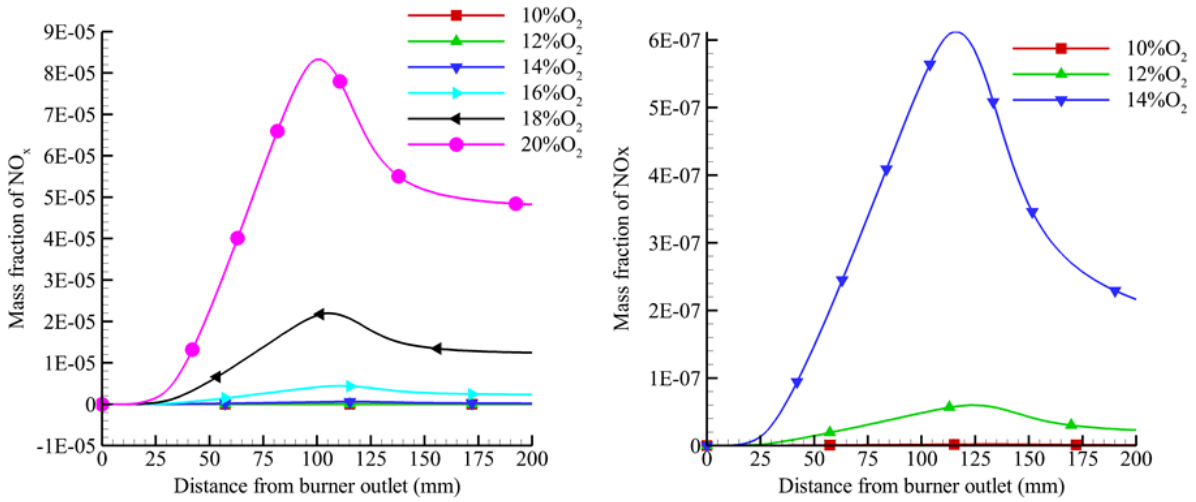


**a)** **b)**

**Figure 12.** Axial $NO_x$ profiles of 80% $CH_4$ – 10% $C_2H_6$ – 10% $N_2$ mixture at; a) 10%-20%, b) 10%-14% $O_2$ concentrations

In distributed regime, although $O_2$ concentration is very low, reaction rates are higher at burner outlet. This is because of increased mass flow rate with $N_2$ and $CO_2$ dilutions (higher turbulence and mixing intensity). However, downstream reaction rate values are higher at $O_2$ rich conditions (Figure 13).

The variations of turbulent rate of reaction, axial and radial temperature values and species distributions of 40% CO – 40% $H_2$ – 20% $CO_2$ and 50% CO – 50% $H_2$ mixtures with $O_2$ addition under flameless distributed combustion conditions are similar in trend to that 80% $CH_4$ – 10% $C_2H_6$ – 10% $N_2$ mixture. Therefore, results obtained from simulations of respective mixtures will not be given in this study. After all, this implies gas composition flexibility of flameless distributed combustion technique.

In Table 2, mean temperature and uniformity index values, and emitted $CO_2$ amounts (from combustor outlet) of 50% CO – 50% $H_2$, 80% $CH_4$ – 10% $C_2H_6$ – 10% $N_2$ and 40% CO – 40% $H_2$ – 20% $CO_2$ mixtures at different $O_2$ concentrations under flameless distributed combustion conditions are tabulated. Irrespective of the gas composition, mean temperature value and uniformity of the thermal field get their highest value at 10% $O_2$ concentration, in other words, at distributed regime. Mean temperature value linearly increases with $O_2$ concentration decrement. Conversely, uniformity index exhibits a non monotonic dependence on $O_2$ concentration. Similar

to the study of Ref. [21], emitted $CO_2$ levels increase based on the both temperature decrement and addition of $CO_2$ to the fresh oxidizer mixture, as $O_2$ amount decreases. In the case of 20 % $O_2$ concentration, emitted $CO_2$ amount is about 2.2 times magnitude of at 10% $O_2$.

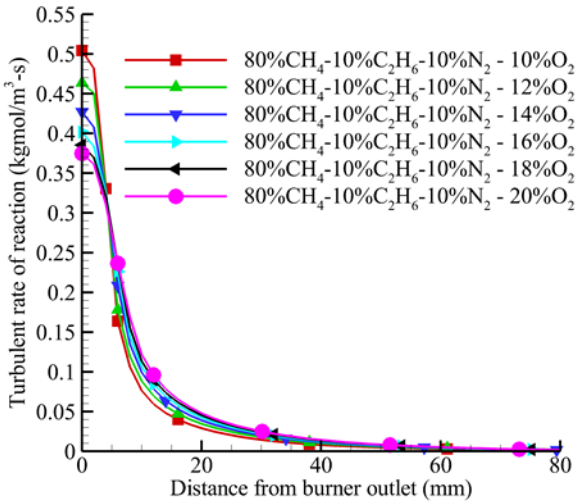


**Figure 13.** Turbulent rate of reaction profiles of 80% $CH_4$ – 10% $C_2H_6$ – 10% $N_2$ mixture at different $O_2$ concentrations

**Table 2.** Mean temperature, uniformity index and emitted $CO_2$ values of 50% CO – 50% $H_2$, 80% $CH_4$ – 10% $C_2H_6$ – 10% $N_2$ and 40% CO – 40% $H_2$ – 20% $CO_2$ mixtures under flameless distributed combustion conditions.

| | **80% $CH_4$ – 10% $C_2H_6$ – 10% $N_2$** | | | **40% CO – 40% $H_2$ – 20% $CO_2$** | | | **50% CO – 50 %$H_2$** | | |
|---|---|---|---|---|---|---|---|---|---|
| **$O_2$ (%)** | Mean Temp. (K) | Uniformity Index | $CO_2$ (kg/s) | Mean Temp. (K) | Uniformity Index | $CO_2$ (kg/s) | Mean Temp. (K) | Uniformity Index | $CO_2$ (kg/s) |
| **10** | 364.42 | 0.9665 | 0.0002382 | 365.67 | 0.9645 | 0.0003337 | 364.33 | 0.9644 | 0.0002561 |
| **12** | 362.78 | 0.9645 | 0.0001959 | 364.18 | 0.9634 | 0.0002984 | 362.80 | 0.9635 | 0.0002195 |
| **14** | 359.71 | 0.9649 | 0.0001621 | 363.21 | 0.9627 | 0.0002705 | 361.39 | 0.9630 | 0.0001951 |
| **16** | 357.81 | 0.9648 | 0.0001371 | 362.14 | 0.9624 | 0.0002521 | 359.89 | 0.9628 | 0.0001769 |
| **18** | 356.49 | 0.9646 | 0.0001192 | 361.08 | 0.9631 | 0.0002365 | 358.41 | 0.9630 | 0.0001603 |
| **20** | 355.22 | 0.9645 | 0.0001051 | 359.99 | 0.9623 | 0.0002257 | 357.06 | 0.9633 | 0.0001491 |

Main challenges associated with oxy-fuel combustion, such as very high flame temperature, high burning velocity, etc. require diluting oxidizer mixture via entrainment of hot combustion products, and this requirement brings in an opportunity to combine oxy-fuel and flameless distributed combustion techniques. Oxy-flameless distributed combustion technique enables a $NO_x$ free exhaust stream which is mainly composed of $CO_2$ and $H_2O$ (easy for carbon capture and sequestration), very low emission levels, and a more uniform temperature distribution [26].

As well as in oxy-fuel and flameless distributed combustion techniques, temperature and species profiles of 50% CO – 50% $H_2$, 80% $CH_4$ – 10% $C_2H_6$ – 10% $N_2$ and 40% CO – 40% $H_2$ – 20% $CO_2$ mixtures throughout the entire combustion chamber concords in trend. Since gas composition versatility of this regime is also proved, predicted results of only 40% CO – 40% $H_2$ – 20% $CO_2$ mixture under oxy-flameless distributed combustion conditions will further be addressed.

At this stage of the study, $O_2$ concentration was reduced from 19% to 11% by a step of 2% ($CO_2$ was added accordingly to simulate injection of product gases), and 40% CO – 40% $H_2$ – 20% $CO_2$ mixture combustion was simulated under 5 different oxidizer atmospheres. When $N_2$ is replaced with $CO_2$ to achieve oxy-flameless distributed combustion conditions, in which $O_2$-$CO_2$ mixture is used as an oxidant, peak temperature values decrease (compared to other combustion techniques), as heat capacity of $CO_2$ is higher than that of $N_2$ [4]. Also, the area of high temperature zone expands. Unlike flameless distributed combustion conditions, temperature profiles at 11% and 19% $O_2$ concentrations coincide in the axial distance range of about 200-800 mm, and then higher exit temperature values form at 11% $O_2$ concentration (Figure 14).

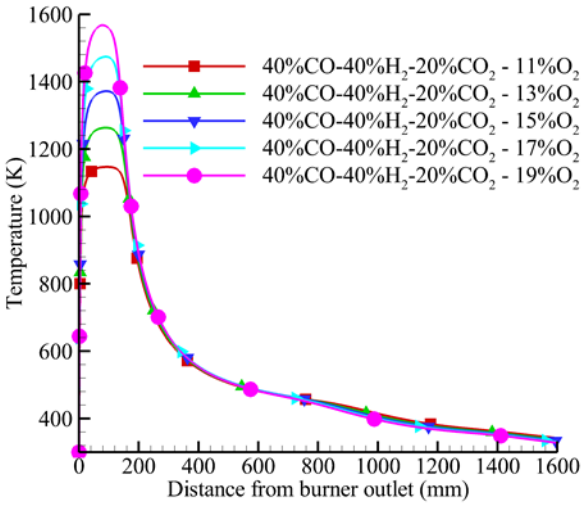


**Figure 14**. Axial temperature profiles of 40% CO – 40% $H_2$ – 20% $CO_2$ mixture at different $O_2$ concentrations

Compared to the oxy-fuel and flameless distributed combustion techniques, radial temperature profiles (at all axial and radial locations) don't differentiate in trend under oxy-flameless distributed combustion conditions. Yet, radial temperature values are the highest at 150 and 250 mm axial locations in spite of the lowest peak temperature values at this combustion regime. This

situation can be attributed to the chemical effects (reaction kinetics are negatively affected, and combustion is completed downstream) of $CO_2$. Lastly, effects of $O_2$ addition on radial temperature values become more distinct at this regime. As $O_2$ amount decreases, radial temperature values decrease more distinctly, and the radial range in which temperature values decrease lengthens with axial distance (Figure 15).

In comparison with flameless distributed combustion technique, mean temperature values are higher at this combustion regime, and uniformity index monotonically increases, as $O_2$ amount decreases (Table 3). Other than these findings, no significant difference in species and reaction rate profiles was observed.

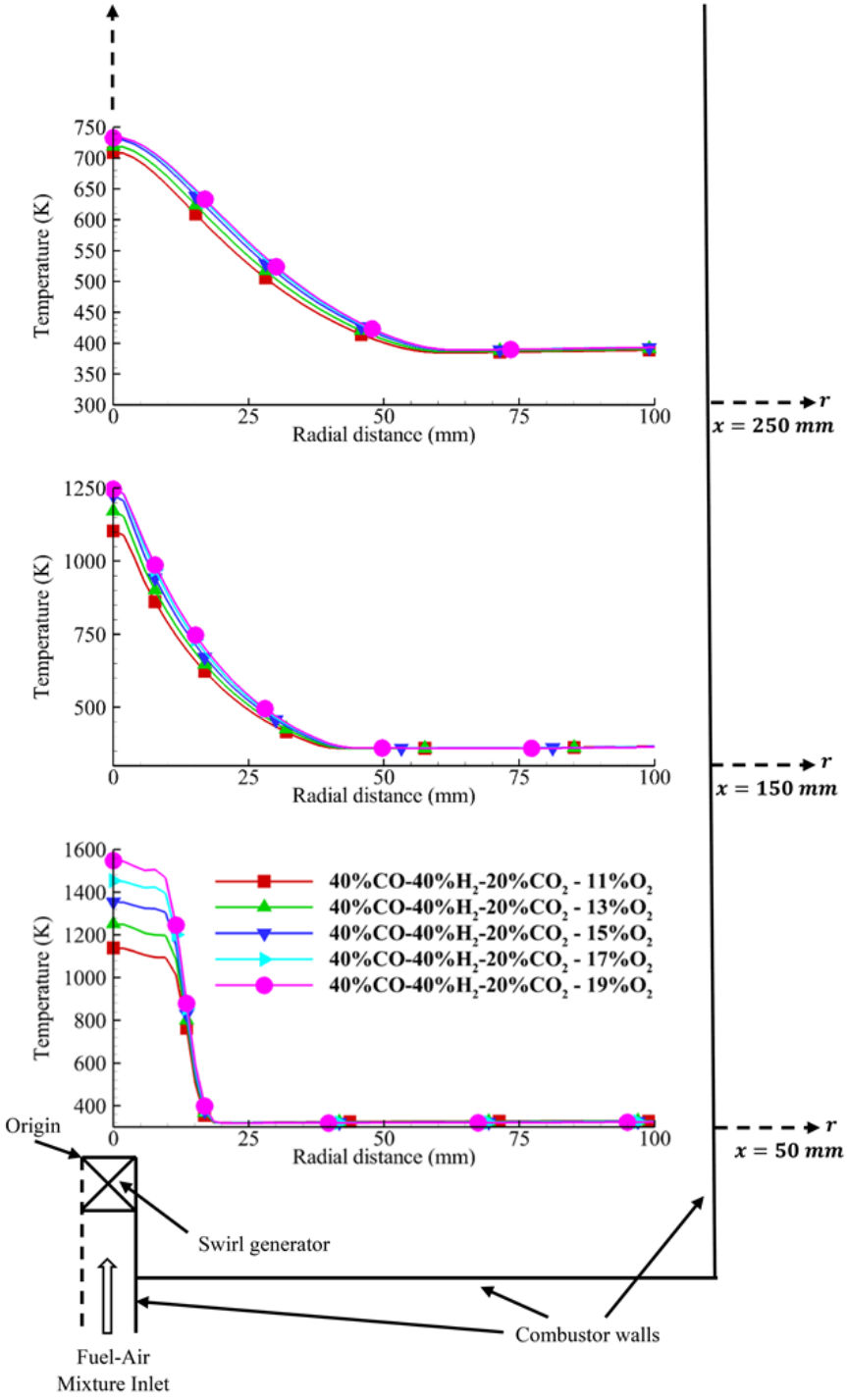


**Figure 15**. Radial temperature profiles of 40% CO – 40% $H_2$ – 20% $CO_2$ mixture at different $O_2$ concentrations

**Table 3.** Mean temperature and uniformity index values of 50% CO – 50% $H_2$, 80% $CH_4$ – 10% $C_2H_6$ – 10% $N_2$ and 40% CO – 40% $H_2$ – 20% $CO_2$ mixtures under oxy-flameless distributed combustion conditions

| | **80% $CH_4$ – 10% $C_2H_6$ – 10% $N_2$** | | **40% CO – 40% $H_2$ – 20% $CO_2$** | | **50% CO – 50 %$H_2$** | |
|---|---|---|---|---|---|---|
| **$O_2$ (%)** | Mean Temp. (K) | Uniformity Index | Mean Temp. (K) | Uniformity Index | Mean Temp. (K) | Uniformity Index |
| **11** | 388.07 | 0.9636 | 388.45 | 0.9604 | 388.91 | 0.9594 |
| **13** | 388.19 | 0.9599 | 387.38 | 0.9579 | 387.87 | 0.9569 |
| **15** | 387.68 | 0.9574 | 387.15 | 0.9558 | 386.07 | 0.9555 |
| **17** | 385.30 | 0.9564 | 385.90 | 0.9547 | 385.20 | 0.9543 |
| **29** | 384.69 | 0.9550 | 384.56 | 0.9541 | 383.53 | 0.9537 |

## 6. CONCLUSION

In this study combustion and emission characteristics of 50% CO – 50% $H_2$, 80% $CH_4$ – 10% $C_2H_6$ – 10% $N_2$ and 40% CO – 40% $H_2$ – 20% $CO_2$ mixtures were investigated under oxy-fuel, flameless distributed and oxy-flameless distributed combustion conditions by using ANSYS Fluent CFD code. To this end, 2D axisymmetric models of an experimentally tested combustor were formed, and premixed combustion of such blends were simulated in these models under different oxidizing atmospheres. During simulation studies, fuel flow rate was not altered to keep thermal load constant at 2 kW. Moreover, equivalence ratio and swirl number were set as 0.8 and 1.0, respectively. To achieve oxy-fuel combustion conditions, $O_2$ concentration in $O_2/CO_2$ mixture was increased from 25% to 50% (by a step of 5%), while $O_2$ concentration was reduced from 19% to 11% (by a step of 2%) for oxy-flameless distributed combustion conditions. Lastly, 90%$N_2$-10%$CO_2$ mixture (the majority of exhaust gases near stoichiometric conditions) was used to dilute combustion air (it was assumed that right amount of air to complete combustion process was initially premixed with fuel), and $O_2$ concentration was reduced from 20% to 10% (by a step of 2%). Some important results are as follows;

Under oxy fuel combustion conditions,

- Peak temperature values increase with $O_2$ concentration. However, slightly lower downstream temperature values form at higher $O_2$ fractions due to the improved heat transfer characteristics at elevated $O_2$ levels. Consistently, Nemitallah and Habib concluded that $O_2$ concentration is an additional parameter in oxy-fuel combustion, which affects combustion characteristics [4].
- Higher radial temperature values occur at lower $O_2$ concentrations starting from a certain axial distance. These temperature values decrease with radial distance, and become insensitive to radial distance from a certain radial location. Nevertheless, the radial range in which temperature values decrease extends, as axial distance increases.

- Oxidizer composition influences flow field, and reaction rate is affected in turn. At high inlet velocities, turbulent mixing improves, hence flame speed increases [12]. Higher turbulent reaction rates at lower $O_2$ fractions near burner outlet are attributed to this phenomenon. But, the opposite is the case for the downstream of the combustor at higher $O_2$ fractions, as there is sufficient amount of $O_2$ to consume fuel molecules, and reaction kinetics are promoted [4].
- Since temperature, species and reaction rate profiles of 50% CO – 50% $H_2$, 80% $CH_4$ – 10% $C_2H_6$ – 10% $N_2$ and 40% CO – 40% $H_2$ – 20% $CO_2$ mixtures similar in trend, above mentioned results are applicable to all mixtures.

Under flameless distributed combustion conditions,

- Compared to the oxy-fuel combustion conditions, dependence of peak temperature values to $O_2$ amount does not considerably alter. However, the axial range with high temperature extends in this regime, as $O_2$ concentration decreases.
- Although there is a big difference in peak temperature values between 10% and 20% $O_2$ concentrations, downstream (200-1600 mm) temperature values are higher at 10% $O_2$ concentration. In accordance with the study of Ref. [16], uniformity increases at high diluent fractions (uniformity is the highest at 10% $O_2$ concentration).
- $NO_x$ emissions dramatically increase, as $O_2$ concentration increases. This increment is not only because of temperature increment, enhanced reaction kinetics and increased $O_2$ amount also cause $NO_x$ to increase [16].
- Khalil and Gupta showed that emissions of $NO_x$ significantly reduce at $O_2$ concentrations lower than 16% [16]. In addition, they also concluded that this value must be about 14.5%, when fuel/air mixture is fed to combustor at room temperature [37]. These values can set a minimum of $O_2$ concentration to obtain flameless distributed combustion conditions. In this study, nearly zero $NO_x$ emissions were obtained at 10% $O_2$ concentration.
- This combustion technique does not depend on gas composition.

Under oxy-flameless distributed combustion conditions.

- High proportion of $CO_2$ in the oxidizer mixture has exceptional impacts on combustion and emission behaviors [38]. Compared to the other combustion techniques, peak temperature values (axial) are lower [4]. But, the area of high temperature zone is the largest at this regime.

- Although peak temperature values are the lowest, radial temperature values are the highest at 150 and 250 mm axial locations, and effects of $O_2$ addition on radial temperature values are more profound at this regime.
- Uniformity of thermal field exhibits a monotonic dependence on $O_2$ concentration at this regime.
- Fuel flexibility of this regime was also proved.

In conclusion, it can be said that these combustion techniques show no significant dependence on gas composition (for the gas compositions studied herein), flameless and oxy flameless combustion techniques enable ultra-low emissions and these techniques are utilizable over a wide gas composition range, and minimum amount of $O_2$ in oxidizer must be ensured to obtain distributed combustion conditions. However, high inlet velocities may bring in some challenges in terms of combustor flow field design [16].

**Acknowledgment**

The author gratefully acknowledges Erciyes University for the use of ANSYS/Fluent CFD code.

**Declaration of Ethical Standards**

The author declares that there is no conflict of interests regarding the publication of this paper.

**REFERENCES**

[1] Li, B., Shi, B., Zhao, X., Ma, K., Xie, D., Zhao, D., & Li, J. "Oxy-fuel combustion of methane in a swirl tubular flame burner under various oxygen contents: Operation limits and combustion instability", *Experimental Thermal and Fluid Science* 2018:90;115-124.

[2] Krieger, G. C., Campos, A. P. V., Takehara, M. D. B., Da Cunha, F. A., Veras, C. G. "Numerical simulation of oxy-fuel combustion for gas turbine applications", *Applied Thermal Engineering* 2015:78;471-481.

[3] Stelzner, B., Weis, C., Habisreuther, P., Zarzalis, N., Trimis, D. "Super-adiabatic flame temperatures in premixed methane flames: A comparison between oxy-fuel and conventional air combustion", *Fuel* 2017: 201;148-155.

[4] Nemitallah, M. A., Habib, M. A. "Experimental and numerical investigations of an atmospheric diffusion oxy-combustion flame in a gas turbine model combustor", *Applied Energy* 2013:111;401-415.

[5] Abubakar, Z., Shakeel, M. R., Mokheimer, E. M. "Experimental and numerical analysis of non-premixed oxy-combustion of hydrogen-enriched propane in a swirl stabilized combustor", *Energy* 2018:165;1401-1414.

[6] Zhong, S., Zhang, F., Peng, Z., Bai, F., Du, Q. "Roles of $CO_2$ and $H_2O$ in premixed turbulent oxy-fuel combustion", *Fuel* 2018:234;1044-1054.

[7] Guan, Y., Han, Y., Wu, M., Liu, W., Cai, L., Yang, Y., Chen, S. "Simulation study on the carbon capture system applying LNG cold energy to the $O_2/H_2O$ oxy-fuel combustion", *Natural Gas Industry B* 2018:5(3);270-275.

[8] Lee, C. E., Lee, S. R., Han, J. W., Park, J. "Numerical study on effect of $CO_2$ addition in flame structure and $NO_x$ formation of $CH_4$-air counterflow diffusion flames", *International Journal of Energy Research* 2001:25(4);343-354.

[9] Glarborg, P., Bentzen, L. L. "Chemical effects of a high $CO_2$ concentration in oxy-fuel combustion of methane", *Energy & Fuels* 2007:22(1);291-296.

[10] Shakeel, M. R., Sanusi, Y. S., Mokheimer, E. M. "Numerical modeling of oxy-fuel combustion in a model gas turbine combustor: Effect of combustion chemistry and radiation model", *Energy Procedia* 2017:142;1647-1652.

[11] Shakeel, M. R., Sanusi, Y. S., Mokheimer, E. M. "Numerical modeling of oxy-methane combustion in a model gas turbine combustor", *Applied Energy* 2018:228;68-81.

[12] Imteyaz, B. A., Nemitallah, M. A., Abdelhafez, A. A., Habib, M. A. "Combustion behavior and stability map of hydrogen-enriched oxy-methane premixed flames in a model gas turbine combustor", *International Journal of Hydrogen Energy* 2018:43(34);16652-16666.

[13] Ditaranto, M., Oppelt, T. "Radiative heat flux characteristics of methane flames in oxy-fuel atmospheres", *Experimental Thermal and Fluid Science* 2011:35(7);1343-1350.

[14] Li, Y. H., Chen, G. B., Wu, F. H., Hsieh, H. F., Chao, Y. C. "Effects of carbon dioxide in oxy-fuel atmosphere on catalytic combustion in a small-scale channel", *Energy* 2016:94;766-774.

[15] Fooladgar, E., Tóth, P., Duwig, C. "Characterization of flameless combustion in a model gas turbine combustor using a novel post-processing tool", *Combustion and Flame* 2019:204;356-367.

[16] Khalil, A. E., Gupta, A. K. "Impact of internal entrainment on high intensity distributed combustion", *Applied Energy* 2015:156;241-250.

[17] Khalil, A. E., Gupta, A. K. "Swirling flowfield for colorless distributed combustion", *Applied Energy* 2014:113;208-218.

[18] Khidr, K. I., Eldrainy, Y. A., EL-Kassaby, M. M. "Towards lower gas turbine emissions: Flameless distributed combustion", *Renewable and Sustainable Energy Reviews* 2017:67;1237-1266.

[19] Khalil, A. E., Gupta, A. K. "Towards colorless distributed combustion regime", *Fuel* 2017:195;113-122.

[20] Karyeyen, S., Feser, J. S., Gupta, A. K. "Swirl assisted distributed combustion behavior using hydrogen-rich gaseous fuels", *Applied Energy* 2019:251;113354.

[21] Karyeyen, S., Ilbas, M. "Application of distributed combustion technique to hydrogen-rich coal gases: A numerical investigation" *International Journal of Hydrogen Energy* 2019:45(5);3641-3650.

[22] Karyeyen, S. "Combustion characteristics of a non-premixed methane flame in a generated burner under distributed combustion conditions: A numerical study", *Fuel* 2018:230;163-171.

[23] Arghode, V. K., & Gupta, A. K. "Investigation of forward flow distributed combustion for gas turbine application", *Applied Energy* 2011:88(1);29-40.

[24] Liu, W., Ouyang, Z., Cao, X., Na, Y. "The influence of air-stage method on flameless combustion of coal gasification fly ash with coal self-preheating technology", *Fuel* 2019:235;1368-1376.

[25] Arghode, V. K., Gupta, A. K. "Investigation of reverse flow distributed combustion for gas turbine application", *Applied Energy* 2011: 88(4);1096-1104.

[26] Khalil, A. E., Gupta, A. K. "The role of $CO_2$ on oxy-colorless distributed combustion", *Applied Energy* 2017:188;466-474.

[27] Karyeyen, S., Feser, J. S., Gupta, A. K. "Hydrogen concentration effects on swirl-stabilized oxy-colorless distributed combustion", *Fuel* 2019:253;772-780.

[28] Yilmaz, H., Yilmaz, I. "Effects of synthetic gas constituents on combustion and emission behavior of premixed $H_2$/CO/$CO_2$/CNG mixture flames", *Journal of the Energy Institute* 2019:92(4);1091-1106.

[29] Li, J., Chou, S. K., Yang, W. M., Li, Z. W. "A numerical study on premixed micro-combustion of $CH_4$–air mixture: Effects of combustor size, geometry and boundary conditions on flame temperature", *Chemical Engineering Journal* 2009:150(1);213-222.

[30] Fluent, A. "12.0 Theory Guide", *Ansys Inc* 2009, 5(5).

[31] Gaikwad, P., Kulkarni, H., Sreedhara, S. "Simplified numerical modelling of oxy-fuel combustion of pulverized coal in a swirl burner", *Applied Thermal Engineering* 2017:124;734-745.

[32] Escue, A., Cui, J. "Comparison of turbulence models in simulating swirling pipe flows", *Applied Mathematical Modelling* 2010:34(10);2840-2849.

[33] Yılmaz, H. "Kaya gazı karışımlarının yanma ve emisyon davranışlarının laboratuvar ölçekli bir yakıcıda sayısal olarak incelenmesi", *Erzincan Üniversitesi Fen Bilimleri Enstitüsü Dergisi* 2020:12(3);1579-1589.

[34] Wu, K. K., Chang, Y. C., Chen, C. H., Chen, Y. D. "High-efficiency combustion of natural gas with 21–30% oxygen-enriched air", *Fuel* 2010:89(9);2455-2462.

[35] Williams, T. C., Shaddix, C. R., Schefer, R. W. "Effect of syngas composition and $CO_2$-diluted oxygen on performance of a premixed swirl-stabilized combustor", *Combustion Science and Technology 2007*:180(1);64-88.

[36] Feser, J. S., Karyeyen, S., Gupta, A. K. "Flowfield impact on distributed combustion in a swirl assisted burner", *Fuel* 2019:263;116643.

[37] Khalil, A. E., Gupta, A. K. "Fuel property effects on distributed combustion", *Fuel* 2016:171;116-124.

[38] Li, S., Xu, Y., Gao, Q. "Measurements and modelling of oxy-fuel coal combustion", *Proceedings of the Combustion Institute* 2019:37(3);2643-2661.